Mapping the neuroanatomy of ABHD16A – ABHD12 enzymes provides new insights into the pathophysiology of PHARC Syndrome.

Introduction

PHARC syndrome is an age dependent genetically recessive neurological disorder primarily marked by a set of 5 symptoms that includes peripheral neuropathy, hearing loss, ataxia, retinitis pigmentosa, and cataract[1-4]. More than 20 mutations have been mapped in *Abhd12* gene in PHARC human subjects. *Abhd12* gene encodes a serine hydrolase enzyme namely α/β – hydrolase containing protein #12 (ABHD12). Extensive biochemical investigations of ABHD12 lead to its annotation as the principal lysophosphatidylserine (lyso-PS) lipase in the mammalian central nervous system (CNS)[5]. ABHD12 knock out (KO) mice accumulate lyso-PS in the neural tissues, followed by elevated microglial cell activation (neuro-inflammation) and sensory motor defects like hearing loss, ataxia and poor coordination, similar to what is observed in PHARC human subjects[5]. This led to the proposal that defective lyso-PS signaling arising out of deregulated lyso-PS metabolism may drive the pathophysiology of PHARC Syndrome. To further map the biosynthetic route of lyso-PS, Kamat et al. annotated ABHD16A as a major lyso-PS biosynthetic enzyme in the mammalian nervous and immune system[6]. These studies fairly established that ABHD16A – lyso-PS – ABHD12 biochemical axis play a crucial role in the mammalian neurophysiology and defects in it can cause pathological conditions like PHARC syndrome. Detailed studies demonstrating the physiological role/significance of lyso-PS in the CNS are unavailable and how defects in lyso-PS metabolism drive PHARC pathophysiology are unclear.

We systematically tried to explore these aspects of the problem and the studies presented here report the extensive molecular characterization of lyso-PS lipid metabolism, flux and signaling in the central nervous system (CNS). We demonstrate the ways in which defective lyso-PS metabolism and signaling drive the pathophysiology of PHARC Syndrome, and opens new avenues towards understanding of neuro-immune disorders. We also describe a few therapeutic intervention strategies to manage the severity of PHARC syndrome. Our studies robustly show that minocycline (a small molecule antibiotic), ABHD16A inhibitor and Toll like receptor #2 (TLR2) inhibitors are very promising small molecules to treat or alleviate severity of PHARC syndrome.

Specific Objectives of the work.

1. Purification and biochemical characterization of ABHD16A (lyso-PS biosynthetic enzyme).
2. Mapping lyso-PS metabolism and flux in the mammalian nervous system.
3. Establishing functional role of lyso-PS in the neuro-immunophysiology and its relation to PHARC pathology.

Material, Methods and Experimental Design.

Materials. All chemicals and salts were brought Sigma until otherwise mentioned. All primary antibodies were brought from Abcam and secondary antibodies from ThermoFisher Scientific until otherwise noted. All the tissue culture reagents were purchased from Hi-Media until stated otherwise.

Animal studies. All animal (mouse) studies described in this paper have received formal approval from Institutional Animal Ethics Committee at IISER Pune (IAEC–IISER Pune) (application numbers: IISER_Pune IAEC/2019_02/07 and IISER_Pune IAEC/2021_01/09), constituted as per the guidelines outlined by the Committee for the Purpose of Control and Supervision of Experiments on Animals (CPCSEA), Government of India. All mice were bred and maintained at National Facility for Gene Function in Health and Disease (NFGFHD), IISER Pune. All mice used in the study were generated by a standard ABHD12 heterozygous x ABHD12 heterozygous or ABHD16A heterozygous x ABHD16A heterozygous breeding scheme and had ad libitum access to food and water. For all the animal studies described here, an equal number of male and female mice (10 – 12 weeks of age were used to control for gender-specific effects if any.

Overexpression and purification of recombinant ABHD16A. The codon optimized human ABHD16A was commercially synthesized and cloned into the pET-22b(+) vector between NdeI and HindIII restriction sites with a C-terminal 6X Histidine-tag for expression in the bacterial host (from Genscript). A sequence verified plasmid with 6X Histidine tag ABHD16A insert was transformed into chemically competent *E. coli* Lemo21 (DE3) cells using heat shock (42 ºC, 30 sec). Temperature, IPTG and *L*-Rhamnose concentrations were screened to get optimal expression of ABHD16A in active form. Overexpression and activity of ABHD16A was checked by resolving membrane proteome on 10% SDS-PAGE gel using activity-based protein profiling (ABPP) gel and Coomassie staining. Overexpressed ABHD16A was solubilized in solubilization buffer containing 20 mM HEPES, 150 mM NaCl, 2 mM SDS or 5 mM lauroylsarcosine sulfate (LSS), pH 7.4. Solubilized ABHD16A was purified using affinity Ni-NTA chromatography and ion exchange chromatography. Purified recombinant ABHD16A was reconstituted in liposomes based artificial membranes.

Substrate assays with purified ABHD16A. 5 µg of purified protein or 20 µg of lysate was incubated with 100-µM-lipid substrate in Dulbecco's phosphate buffered saline (DPBS) at 37°C, 30 mins with constant shaking. Reaction mixture was quenched with 250 µL of 2:1 $CHCl_3$/MeOH containing 1 nmol of 17:1 free fatty acid (FFA) and 17:1 lysophosphatidylserine (lyso-PS) as internal standards. Lipids from the reaction mixture were extracted using Folch’s extraction and extracted lipids were analyzed using liquid chromatography coupled mass spectrometry. Area under the curve for lipids were normalized to that of 17:1 free fatty acid or 17:1 lyso-PS internal standard. Normalized values obtained from last step were further normalized with time of the reaction and amount of the proteome used.

Tissue culture and lipid treatments to cells. Cells were cultured in Dulbecco's Modified Eagle Medium (DMEM) (HiMedia) with 10% (v/v) Fetal Bovine Serum (Thermo Fischer Scientific) and 1X penicillin streptomycin (MP Biomedicals) at 37 °C, 5% (v/v) CO_2. Cells were counted using trypan blue method on a BTC20 automated cell counter (Bio-Rad) as per as manufacturer's instructions. Cells were seeded in 35 mm tissue culture dish at 3 x 106 and cultured for 24 h, washed with sterile DPBS (3x) and treated with Lyso-PS 18:0 solubilized in serum free DMEM media.

Cellular fractionation studies. Cells were harvested from 2 x 15 cm tissue culture plates or half mice brain (from mice 8-10 weeks old) was collected washed with ice-cold DPBS - HIMEDIA, pH 7.4, and homogenized in 3 mL of ice-cold 250-STM homogenization buffer (containing 250 mM sucrose, 50 mM Tris-HCl (pH 7.4), 5 mM $MgCl_2$, 1 mM DTT, 25 µg/mL spermine and 25 µg/mL spermidine, 1 mM PMSF) until isolated floating nuclei were seen under the phase contrast microscope. The unlysed cells were pelleted at 200 g for 3 mins at 4 °C and resulting supernatant was centrifuged at 1000 g for 15 mins at 4 °C to pellet the nuclear fraction. The supernatant from this step, was centrifuged at 10,000 g for 15 mins at 4 °C to pellet mitochondrial enriched fraction. Left over supernatant was centrifuged at 100,000 g for 60 mins at 4 °C to pellet microsomes and supernatant was collected as soluble cytoplasmic fraction. Mitochondrial enriched fraction was further purified by re-suspending it in 2M-STMDPS buffer (2 M sucrose, 50 mM Tris-HCl (pH 7.4), 5 mM $MgCl_2$, 1 mM DTT, 25 µg/mL spermine and 25 µg/mL spermidine, 1 mM PMSF) and centrifuged it at 6,000 g for 15 mins at 4 °C to pellet a pure mitochondrial fraction. Each pellet fraction was re-suspended in DPBS and protein was estimated using Bradford reagent (Sigma-Aldrich). Proteome from each fraction was denatured by boiling with 4X loading dye at 95 °C for 15 mins and denatured proteome was separated over 10% SDS-PAGE gel and used for western blot.

Primary neuronal culture. Brain was dissected out of E18 mice embryos and meninges were stripped under the stereotaxic microscope. Thereafter, dissected brains were minced in DMEM supplemented with 10% (v/v) heat inactivated FBS and 1X antibiotic-antimycotic solution. Minced tissue was trypsinized with 0.25% (w/v) Trypsin for 10 mins over ice and incubated with DNAse (0.1 mg/ml) for 5 mins over ice. Cells were pelleted down by spinning at 300 g for 3 mins and washed with Hank's Balanced Salt Solution (2X). Cells were re-suspended in DMEM supplemented with 10% (w/v) heat inactivated FBS and 1X antibiotic-antimycotic solution and plated on Poly-D-lysine coated coverslips or plates. Cells were allowed to adhere to tissue culture plate for 3 hat 37 °C, 5% (v/v) CO_2. Thereafter, culture media was changed to Neurobasal Medium supplemented with 1X antibiotic-antimycotic, 1X B-27 (Thermo-Scientific), 1X Glutamine (Gibco) at 37 °C with 5% (v/v) CO_2. Cells were grown for 14 days and media was changed every alternate day to achieve healthy differentiated neurons.

Animal studies. All mouse studies described in this chapter received formal approval from the Indian Institute of Science Education and Research, Pune-Institutional Animal Ethics Committee (IISER-P IAEC), under the guidelines outlined by the Committee for the Purpose of Control and Supervision of Experiments on Animals (CPCSEA), Government of India. All mice were maintained at National Centre

for Gene Function in Health and Disease. All mice used in the study were generated by breeding either ABHD12 heterozygous (het) mice or ABHD16A het mice and had *ad libitum* access to water and food.

Western blot analysis. Denatured proteome (40-50 µg) was resolved over 10% SDS-PAGE gel and transferred to methanol activated PVDF membrane (GE Healthcare) at 60V for 12 h at 4 °C. Post-transfer, membrane was blocked with 5% (w/v) milk or bovine serum albumin (BSA) in DPBS, pH 7.4 containing 0.1% (w/v) Tween 20 (DPBST), and subsequently incubated with primary antibody (1:1000 dilution in 5% (w/v) milk in DPBST) overnight at 4 °C. Membrane was washed with DPBST (5X) at 25 °C and incubated with secondary antibody (1:10,000 dilution in 5% (w/v) milk (BSA) in DPBST) for 90 mins at 25 °C. Thereafter, membrane was washed in DPBST (5x) at 25 °C and developed using Thermo West Pico western blotting substrate (Thermofisher Scientific) and visualized using Syngene G-Box Chemi-XRQ gel documentation system.

Immunohistochemical analysis. Mice were deeply anaesthetized using isoflurane and subsequently perfused with chilled phosphate buffer saline (PBS) followed by 4% (w/v) paraformaldehyde. Brains were dissected out and left in 4% (w/v) paraformaldehyde overnight at 4 °C and then transferred into 30% (w/v) sucrose in PBS until brains sank to the bottom of the tubes (~ 3 days). Coronal 25 µm sections were cut on a freezing microtome maintained at -30 °C, and sections were collected in ice-cold PBS. For 3, 3'-diaminobenzidine (DAB) based bright field immunohistochemistry (IHC), endogenous peroxidases were inactivated with 3% (v/v) hydrogen peroxide in PBS for 15 min at 25 °C in dark. Thereafter the sections were washed twice with 1% (w/v) BSA in PBS and permeabilized with 0.1% (v/v) Triton X-100 and 0.5% (w/v) BSA in PBS for 45 mins at 25 °C. The sections were then incubated with primary antibody in 1% (w/v) BSA overnight at 4 °C. Following overnight incubation, the sections were washed three times with 0.5% (w/v) BSA in PBS and incubated with secondary antibody, biotinylated horse-anti rabbit [Vector labs, BP-1100] or biotinylated goat-anti mouse [Vector labs, BP-9200] in 0.5% (w/v) BSA in PBS for 1 h at RT. Following this treatment, the sections were washed twice in 0.5 % (w/v) BSA in PBS, incubated with ABC Elite Vectastatin (Vector labs, PK-6100) for 1 h at RT and subsequently washed twice with excess PBS. Finally, the sections were stained with ImmPACT DAB (Vector labs, SK-4105) for 3 min in dark, transferred to excess PBS and mounted with VectaMount Mounting Medium (Vector labs, H-5000) using glass slides and coverslips. For confocal laser scanning based IHC, collected sections were directly permeabilized with 0.1% (v/v) Triton X-100 and 0.5% (w/v) BSA in PBS for 45 mins at 25 °C and block with 1% (w/v) BSA in PBS for 1 h at 25 °C. Thereafter, sections were washed with 0.5% (w/v) BSA in PBS (3X) and incubated with primary antibody for 16 h at 25 °C. Sections were washed in 0.5% (w/v) BSA in PBS (3X) and incubated with secondary antibody (1:1000 dilution) for 60 mins at 25 °C. Sections were washed in excess PBS and mounted on glass slides with Fluoromount™ aqueous mounting medium (Sigma Aldrich).

Quantitative lipid measurements. Mice were anesthetized with isoflurane and subsequently sacrificed with cervical dislocation. Thereafter, different regions of the mice brain were micro dissected within a minute and flash frozen in liquid nitrogen. Brain regions were weighed for their wet weight and lipids

were extracted based on Folch's lipid extraction method. Briefly, dissected regions were washed with chilled DPBS (3X) and homogenized in 6 mL of chilled 2:1:1 (vol/vol/vol) $CHCl_3$/MeOH/DPBS with 1 nmol of internal standard (37:4 PS and 17:1 lyso-PS). The mixture was centrifuged at 2,800 g for 15 mins and bottom organic layer was collected and the aqueous phase was acidified with 50 µL of formic acid. Acidified aqueous phase was vortexed, volume was adjusted to 6 mL with $CHCl_3$ and centrifuged at 2,800 g for 15 mins and bottom organic layer was collected. Organic extracts from both the steps were pooled and dried under inert N_2-stream gas. Dried lipid extract was re-suspended in 200 µL of 2:1 (v/v) $CHCl_3$/MeOH and 20 µL of it was injected for targeted LC-MS/MS analysis. Lipids were separated on Gemini 5U C18-reverse phase column (Phenomenex). LC solvents were as follows: - Solvent A, 95:5 (v/v) H_2O/MeOH + 0.1% (v/v) NH_4OH, Solvent B, 60:35:5 (v/v/v) IPA/MeOH/H_2O + 0.1% (v/v) NH_4OH. All lipids were quantified with established multiple reaction monitoring high resolution (MRM-HR) method on Sciex X500R QTOF instrument coupled to an Exion-series UPLC with quaternary pump. Data collected over the instrument was analyzed using SciexOS software. MS parameters were as follows: - ESI mode of ionization, curtain gas 1 = 60, curtain gas 2 = 40, ion spray voltage = -5,500 V, temperature = 550°C. All quantifications were done by calculating area under the curve and normalizing it to the area under the curve for respective internal standard and weight of the wet tissues.

Phosphoblot analysis. Cells were washed and scraped in DPBS supplemented with phosphatase inhibitors (1 mM sodium pyruphosphate, 1 mM sodium orthovandate, 1 mM sodium fluoride, 1 mM β-glycerophosphate). Cells were lysed on ice using lysis buffer constituting 1 mM of sodium pyrophosphate, sodium orthovandate, sodium fluoride, β-glycerophosphate and 1% (v/v) Triton X-100. Proteome was denatured by boiling it in 4X SDS loading dye and separated over 10% SDS-PAGE gel. Thereafter, it was processed for western blot as described under western blot section.

Statistical analysis. All data in this paper was plotted and statistically analyzed using the Prism 9 (version 9.1.0) software for macOS (GraphPad). All bar data in this paper is represented as the mean □standard deviation (SD) from at least three independent biological replicates per experimental group. The Student's two-tailed unpaired parametric t-test was used to determine the statistical significance between different experimental groups, and a p-value of < 0.05 was considered statistically significant in this study.

Results

ABHD16A is a phosphatidylserine specific phospholipase A_2 type enzyme. We assayed ABHD16A (using ABHD16A overexpressing HEK membrane proteoliposomes leveraging mock transfected HEK membrane proteoliposomes) for its lipase activity against commercially available phospholipids like phosphatidylserine (PS), phosphatidylcholine (PC), phosphatidylglycerol (PG), phosphatidylethanolamine (PE) and found that ABHD16A dependent hydrolase activity for PS was 3-4 fold higher compared to other phospholipids that includes phosphatidylcholine (PC), phospahtidylethanolamine (PE), phosphatidylglycerol (PG), phosphatidylinositol (PI) and plasmalogens

(**Fig. 1A**). Next, we asked if ABHD16A cleaves sn-1 or sn-2 ester bond on the glycerol backbone PS lipids. Towards this, set up a mass spectrometry dependent phospholipase assay for purified wild type (WT) ABHD16A and active site serine to alanine S355A mutant ABHD16A and, in my lipase assays sn-2 FFA and sn-2 lyso-PS were released, with absolutely no signs of sn-1 FFA or sn-1 lyso-PS release. It primarily suggested that ABHD16A cleaves sn-2 ester bond and acts as PS specific phospholipase A_2 enzyme (**Fig. 1B-D**). ABHD16A activity generates sn-2 lyso-PS (**Fig. 1D**), which is a potent signaling molecule in the peripheral tissues like mast cells but its physiological significance in CNS remains unknown, despite its established link to neurological disorders like PHARC and neuropathic pain.

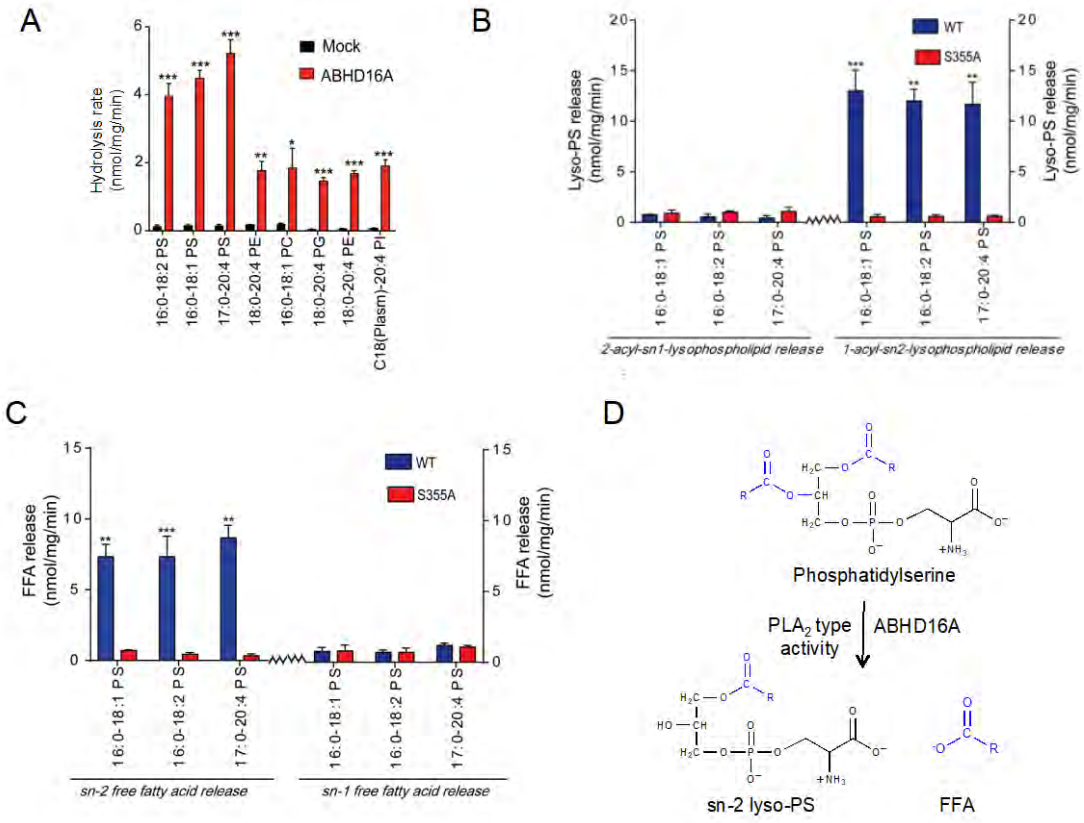

*Fig.1: Phospholipase assay shows that ABHD16A is a PS-specific PLA_2 enzyme. A – ABHD16A prefers PS to other phospholipids like PC, PE, PG and PI. B – Lyso-PS release measurements shows sn-2 lyso-PS release as a function of ABHD16A activity. C – FFA release measurements shows sn-2 FFA release as a function of ABHD16A activity. D – Reaction scheme showing PLA_2 type lipase activity of ABHD16A. Data plotted as mean ± standard deviation. Student's t-test (two-tailed): **P<0.01, ***P<0.001, ****P<0.0001.*

ABHD16A and ABHD12 regulate lyso-PS flux from the endoplasmic reticulum of the mammalian cells. To understand the flux of lyso-PS lipids in the mammalian cells, we aimed to map the expression and localization of lyso-PS metabolic enzymes ABHD16 and ABHD12. Since, these lipases are most abundant in the neural tissues, we fractionated subcellular components of the mice brain and probed for ABHD16A and ABHD12 in their lysates using western blots (**Fig. 2A**). WE isolated cytoplasm, microsomes (primarily plasma membrane and endoplasmic reticulum), mitochondria and nucleus from

the mice brain. These fractions were approximately 90% pure as assessed by probing for organelle specific markers on the western blot (anti-ATP5a for mitochondria, anti-Calnexin for ER, anti-Lamin for nucleus, anti-PMP70 for peroxisomes, anti-GM130 for Golgi, and anti-Actin for cytosol) (**Fig. 2A**).

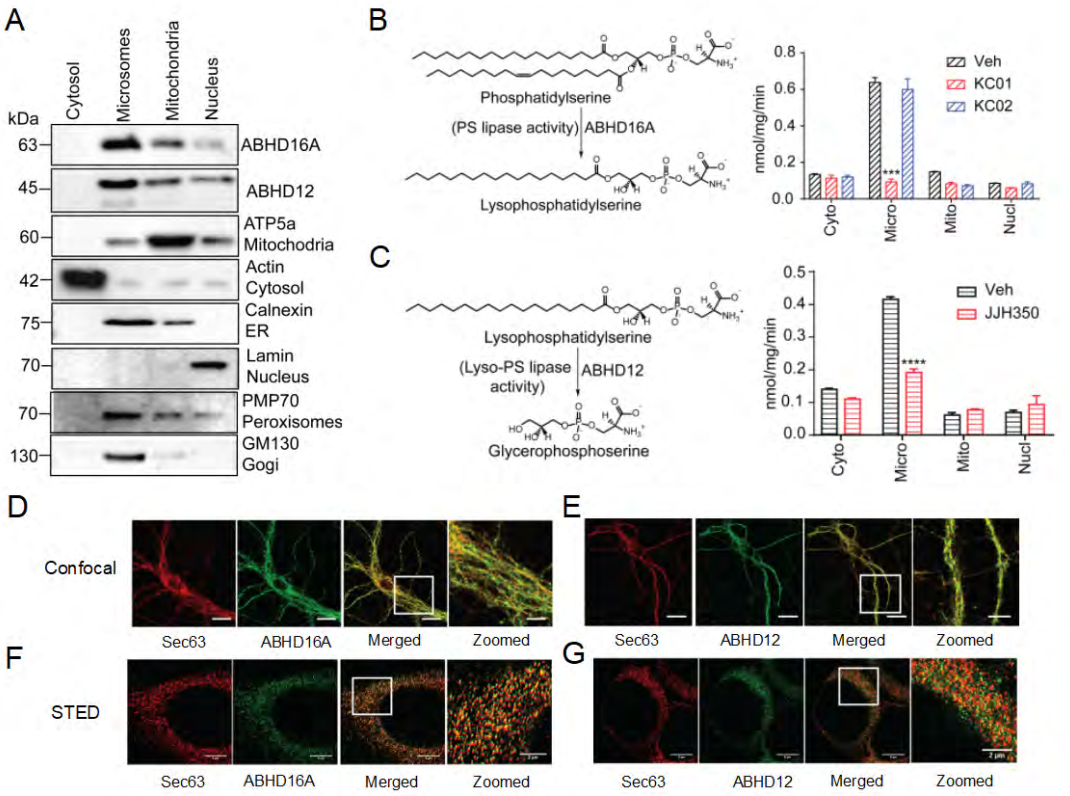

*Fig.2: ABHD16A and ABHD12 regulate lyso-PS from the ER in the mammalian cells. A – Western blot probing ABHD16A and ABHD12 in the subcellular fractions of the brain. B – PS lipase activity on subcellular fractions of the brain. KC01 – specific inhibitor for ABHD16A. KCO2 is an inactive structural control or KC01. C – Lyso-PS lipase activity on subcellular fractions of the brain. JJH350 – specific inhibitor for ABHD12. D and E – Representative confocal microscopy image showing ABHD16A (D) and ABHD12 (E) colocalization with Sec63 – ER marker. F and G – Representative STED microscopy image showing ABHD16A (F) and ABHD12 (G) colocalization with Sec63 – ER marker. Data plotted as mean ± standard deviation. Student's t-test (two-tailed): **P<0.01, ***P<0.001, ****P<0.0001.*

WE found that both ABHD16A and ABHD12 are enriched in the microsomes of the mice brain that primarily consist of endoplasmic reticulum (anti-Calnexin) **(Fig. 2A)**. Next, WE measured PS-lipase activity (for ABHD16A) using PS 18:0-18:1 as substrate on isolated organelle fractions from the brain (**Fig. 2B**). PS-lipase activity was maximal in the microsomal fractions of the mouse brain (**Fig. 2B**) and treatment with KC01 – an active ABHD16A inhibitor, significantly inhibited PS-lipase activities in the microsomal fractions of mouse brain (**Fig. 2B**) but it was largely unaffected on treatment with KCO2 – an inactive structural analog of KC01 (**Fig. 2B**). This established that PS lipase activity on microsomes is largely coming from ABHD16A activity. Next, we tested these organelle fractions for lyso-PS lipase activity (for ABHD12) assay using lyso-PS 18:0 as a substrate (**Fig. 2C**) and found that lyso-PS activity

is also maximal in the microsomal fractions of the mouse brain (**Fig. 2C**) and it was largely ablated on treatment with JJH350 – a specific inhibitor of ABHD12 (**Fig. 2C**), suggesting that lyso-PS lipase activity on microsomes was coming from ABHD12. Since, microsomal fractions typically consists of ER, plasma-membrane peroxisomes and other cellular vesicles, in the next step WE used immunofluorescence assay and co-localization microscopy to probe the localization of ABHD16A and ABHD12. WE isolated primary cortical neurons from the mice embryos and differentiated them in tissue culture. Confocal microscopy based immunofluorescence studies showed that both ABHD16A and ABHD12 co-localize with an endoplasmic reticulum marker – Sec63 (**Fig. 2D,E**). WE also confirmed localization of these lipases at ER using stimulated emission depletion (STED) super resolution microscopy (**Fig. 2F,G**). To make sure that localization of ABHD16A and ABHD12 is generic, we probed their subcellular localization in mammalian secondary cell lines (namely, Neuro-2a, MCF7, and COS7 cells) and they were localized consistently at ER across all tested cell lines (data not shown).

Mapping ABHD16A–ABHD12 activity across brain regions suggests its important activity in the cerebellum. Having mapped the subcellular flux of lyso-PS, it was interesting to map the lyso-PS flux in the mammalian central nervous system. Since, defective lyso-PS metabolism and its accumulation are speculated to drive the pathophysiology of PHARC syndrome. We were curious to check if defects in lyso-PS flux can be mapped to specific brain regions and if we can relate it to the neural defects that we see in the PHARC human subjects. First, we micro-dissected different regions of the adult mice brain namely – olfactory bulb (OB), prefrontal cortex (PFC), cortex (Ctx), hippocampus (Hippo), thalamus (Thala), and cerebellum (Cereb). We probed for ABHD16A and ABHD12 in the lysates of dissected brain regions using western blot. We found that ABHD16A is approximately 3 fold more enriched in the cerebellum (**Fig. 3A,B**) compared to other regions of an adult brain. ABHD16A was 2 approximately 1.5 fold higher in olfactory bulb compared to other brain regions but approximately 2 fold lower than in the cerebellum (**Fig. 3A,B**). ABHD12 was ubiquitous in expression across the mice brain regions with approximately 1.5 fold higher expression in cortex and hippocampus but it was not as distinctly localized as ABHD16A. (**Fig. 3A,B**). To complement the lipase abundance data, we also measured PS lipase activity and lyso-PS lipase activity in the dissected brain regions. Consistent with the western blots, PS lipase activity (ABHD16A – principal brain PS lipase) was highest in the cerebellum whereas lyso-PS lipase activity (ABHD12 – principal lyso-PS lipase) was ubiquitous across brain regions (**Fig. 3C**). Next, we measured lyso-PS in different brain regions and consistent with ABHD16A-ABHD12 abundance and activity, we found that lyso-PS species were most abundant in the cerebellum followed by olfactory bulb (**Fig. 3D**). In next step, we quantified the disturbances in lyso-PS levels across brain regions when ABHD16A or ABHD12 activity is lost using ABHD16A KO and ABHD12 KO mice respectively. We found that loss of ABHD16A activity led to severe reduction in lyso-PS levels primarily in the cerebellum followed by olfactory bulb (**Fig. 3E**). Loss of ABHD12 activity led to the massive build up of lyso-PS across brain regions but changes were 4-5 fold higher in the cerebellum (**Fig. 3F**). These studies largely suggested that perturbations in the ABHD16A-ABHD12 activity causes major changes in cerebellum, underscoring some pivotal role of lyso-PS in the cerebellar region.

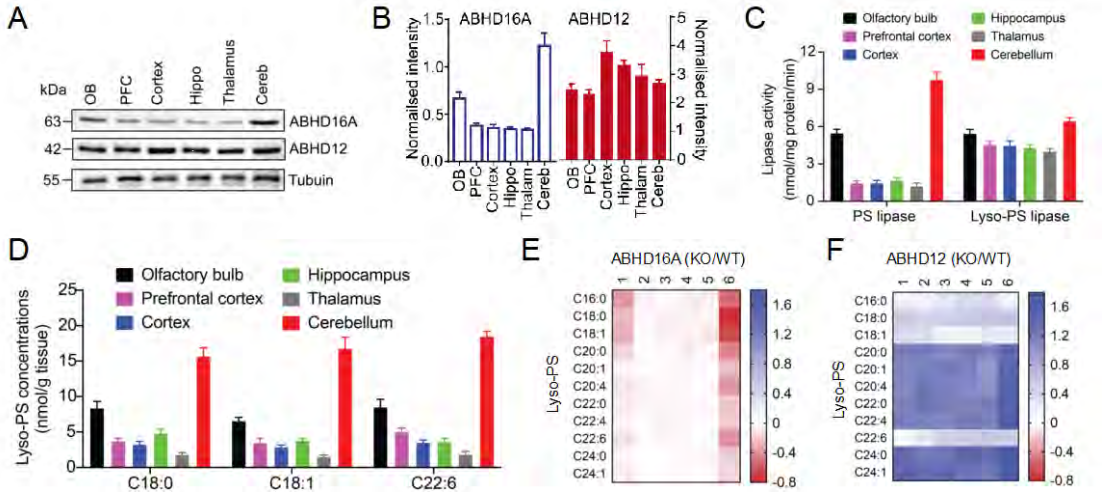

Fig.3: Mapping ABHD16A–ABHD12 activity across brain regions suggests its important activity in the cerebellum. A – Representative western blot probing ABHD16A and ABHD12 abundance across brain regions. B – Blot quantitation of ABHD16A and ABHD12 in different brain regions. C – PS lipase and lyso-PS lipase activity across brain regions. D – Lyso-PS abundance across different brain regions. E – Changes in lyso-PS levels across brain regions on loss of ABHD16A activity. F – Changes in lyso-PS levels across brain regions on loss of ABHD12 activity. 1-olfactory bulb, 2- prefrontal cortex, 3-cortex, 4-hippocampus, 5-thalamus, 6-cerebellum. Data plotted in E and F is on log_{10} scale value of lyso-PS levels in KO/WT. Data plotted as mean ± standard deviation.

ABHD16A – ABHD12 activity regulated lyso-PS modulates granule neuron – Purkinje neuron communication in cerebellum. Since, ABHD16A, ABHD12 and lyso-PS measurements suggested its differential abundance in the cerebellum, as a next step, we used immunohistochemistry to map the cell specific expression of ABHD16A and ABHD12 in the brain. ABHD16A was highest expressed in the cerebellum (**Fig. 4A**), whereas ABHD12 was expressed across all brain regions (**Fig. 4B**). Interestingly, in the cerebellum ABHD16A and ABHD12 were expressed on the different layers of the cerebellum. ABHD16A was highly expressed in granular layer whereas ABHD12 was highly expressed in the ganglionic layer of the cerebellum (**Fig. 4 A,B**). Granular layer typically hosts granule neurons whereas ganglionic layer hosts the Purkinje neurons. To confirm this cell specific expression of ABHD16A and ABHD12 in cerebellum, we performed immunofluorescence assay on the brain slices. ABHD16A was highly expressed on the granule neurons of the cerebellum – marked by NeuN antibody whereas ABHD12 was almost exclusively enriched in the Purkinje neurons marked by Calbindin antibody (**Fig. 4C**). Based on differential expression, we proposed that lyso-PS might act a signaling molecule in granule neuron to Purkinje neuron communication since this pair of neurons are established to cross in the neuroscience literature (**Fig. 4D**).

ABHD16A – ABHD12 activity regulated lyso-PS modulates granule neurons – Purkinje neuron communication in cerebellum. Next, we decided to test the hypothesis that lyso-PS can act as a

signaling molecule between granule and Purkinje neurons. First, we tested the effects of lyso-PS on secondary

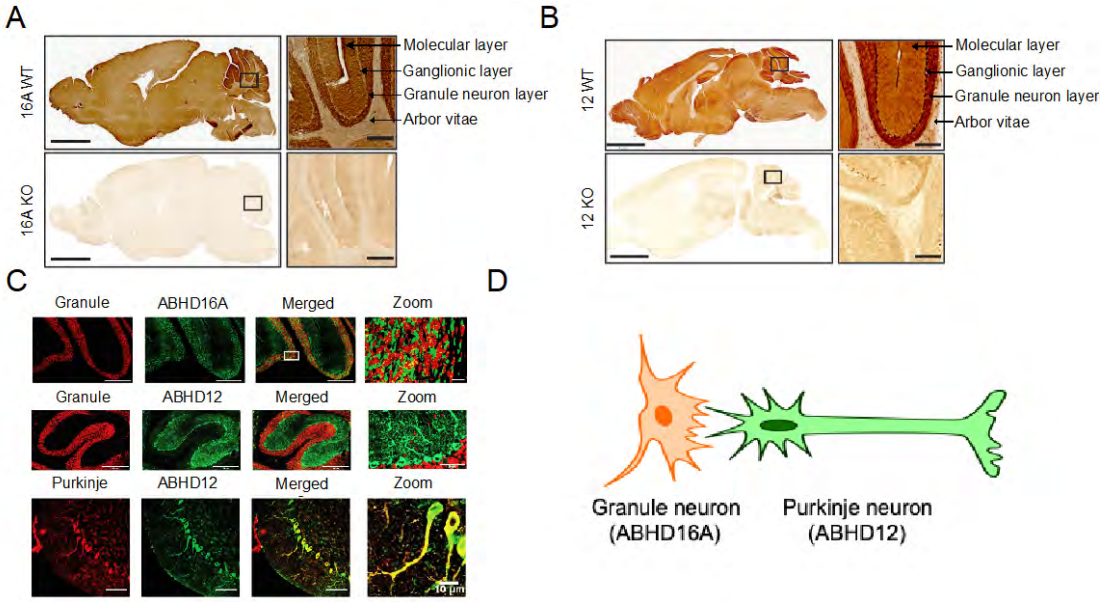

Fig.4: ABHD16A and ABHD12 are differentially enriched in the cerebellum. A – Representative IHC image for ABHD16A staining in the adult mice brain. B – Representative IHC image for ABHD12 staining in the adult mice brain. C – Immunofluorescence assay showing ABHD16A expression on granule neurons (Anti-NeuN) and ABHD12 expression on Purkinje neurons (anti-Calbindin). ABHD12 didn't co-localize in the granule neurons (anti-NeuN). D – Proposed scheme of granule neuron Purkinje neuron cross talk for lyso-PS metabolism and signaling.

neuronal cell lines which act as surrogate for neurons and are easy to maintain and culture. Lyso-PS 18:0 is the most abundant lyso-PS in the brain; hence we used lyso-PS 18:0 as a model lyso-PS to screen for phosphorylation pathways. We found that lyso-PS 18:0 treatment to Neuro-2a cell lines inducing phosphorylation of ERK1/2 (pERK1/2) within 15-mins and phosphorylation state was maintained till 30 mins (**Fig. 5A),** whereas corresponding free fatty acid control (FFA 18:0) didn't bring any changes in pERK1/2 levels (**Fig. 5B**), suggesting that ERK1/2 phosphorylation is indeed induced by lyso-PS 18:0 not by degraded free fatty acid product of the lyso-PS. Since, lyso-PS is not a individual molecule, instead it is a library of naturally existing lipids, we screened synthetic lyso-PS library with different fatty acids appended to them. We found that long chain lyso-PS (i.e. lyso-PS 16:0, 18:0, 20:0) were more potent in inducing phosphorylation of ERK1/2 in Neuro-2a cells (**Fig. 5C**) compared to mid chain lyso-PS (i.e. lyso-PS 10:0, 12:0, 14:0) or very long chain lyso-PS (lyso-PS 22:0, 24:0) in similar time points tested (up to 45 mins). Lyso-PS was the most potent among all lyso-PS and this observation is interesting to the fact pointed before i.e. lyso-PS 18:0 is the most abundant lyso-PS in the mammalian CNS. We also looked for changes in other phosphorylation pathways like phospho-tyrosine and phospho-Akt1, etc. but lyso-PS treatments didn't bring any change in the phosphorylation of tyrosine or Akt1 in Neuro-2a cells (Data not shown). Having confirmed that lyso-PS acts as a signaling molecule in the neurons and induces activation of ERK1/2 phosphorylation mediated signal transduction pathways.

Next, we moved on to test this in Purkinje neurons, we cultured primary cerebellar neurons from E18 embryos and treated them with lyso-PS 18:0. In the microscopy based immunofluorescence assay, we found that levels of phosphorylated ERK1/2 were ~2 fold higher in the lyso-PS treated set of Purkinje neurons (located and marked by Calbindin staining) compared to vehicle treated cells (**Fig. 5D**). ABHD12 KO mice have several fold higher lyso-PS in the cerebellum compared to its WT littermate, so, next, we asked if Purkine neurons in the ABHD12 KO mice have basally higher pERK1/2 levels. In the adult ABHD12 KO mice brain, we found that pERK1/2 levels were ~1.5-2 fold higher compared to that in the Purkinje neurons of adult ABHD12 WT mice (**Fig. 5E**).

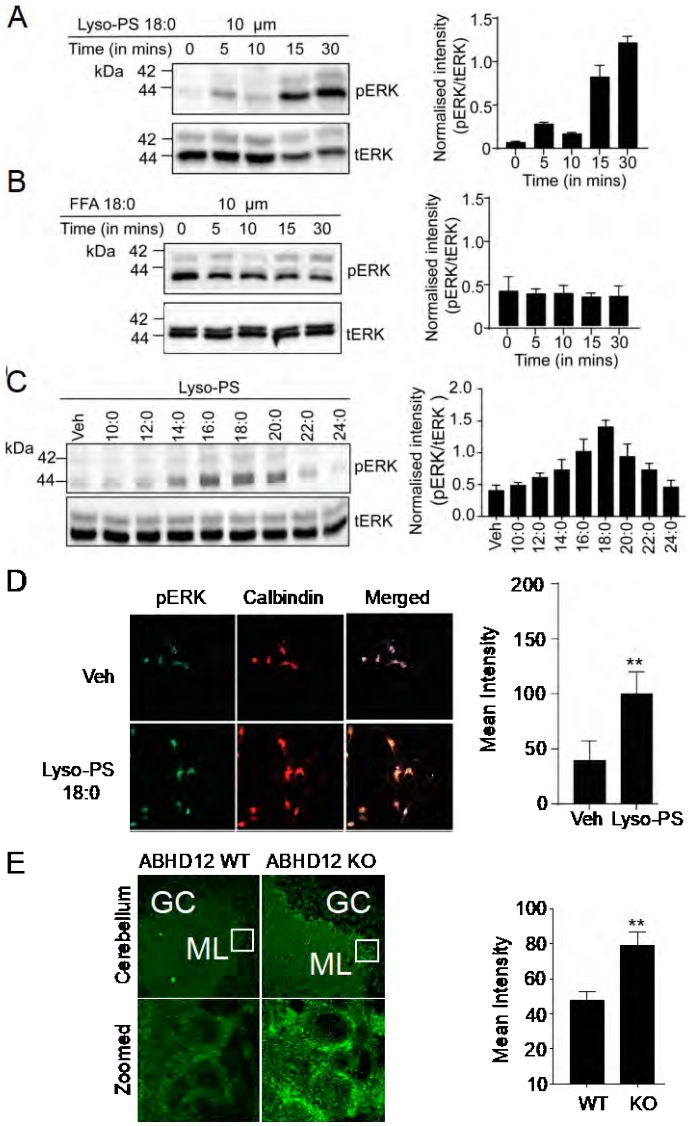

Fig. 5: Lyso-PS acts as a paracrine-signaling molecule between granule and Purkinje neurons. A – Lyso-PS 18:0 induced ERK1/2 phosphorylation in Neuro-2a cells. B – Free fatty acid 18:0 did not induce any visible ERK1/2 phosphorylation in Neuro-2a cells. C – Representative blot showing long chain lyso-PS (lyso-PS 16:0, 18:0, 20:0) were more potent in inducing ERK1/2 phosphorylation than mid chain (lyso-PS 10:0, 12:0, 14:0) or very long chain lyso-PS (lyso-PS 22:0, and 24:0). D – Lyso-PS 18:0 treatment induced ERK1/2 phosphorylation in primary Purkinje neurons. E – Purkinje neurons in ABHD12 KO mice

*brain slice show elevated levels of pERK1/2 compared to their WT littermates. GC - Granular layer, ML – Molecular layer. All plotted values on y-axis are ration of phospho-ERK (pERK1/2) to total ERK (tERK1/2). Data plotted as mean ± standard deviation. Student's t-test (two-tailed): **P<0.01, ***P<0.001, ****P<0.0001.*

ABHD12 activity modulates microglial cell physiology in the brain. It was previously reported that loss of ABHD12 activity leads to the lyso-PS accumulation succeeding which microglial cells are activated especially in the cerebellum[5]. My localization and lipidomics experiments too suggest some crucial physiological role of ABHD12 and lyso-PS in the mammalian cerebellum. Here, we leveraged ABHD12 KO mice along with their WT littermates to investigate the role of lyso-PS in the microglial cell physiology. First, we probed for the microglial cells (using anti-Iba1 antibody); we didn't find any morphological changes in microglial cells of WT and ABHD12 KO mice <5-6 months old. Microglial cells in ABHD12 KO mice >1 year old showed significant elevation in their activation state (i.e. soma size >200 μm^2) (**Fig. 6A,B**). It suggested some role of ABHD12 and lyso-PS in the neuro-immunophysiology. To investigate any such role, We immune challenged WT and ABHD12 KO mice using lipopolysaccharide (LPS) at the dose of 10 mg/kg body weight for 6 hours and looked at their microglial cell morphology. On acute immune challenge, cerebellum of ABHD12KO mice had slightly more number of activated microglial cells compared to their WT controls but this increase failed to reach statistical significance (data not shown). On acute immune challenge, microglial cells of ABHD12 KO mice showed larger soma and complete retraction of their dendrites, adopting amoeboid morphology compared to their LPS treated WT littermates (**Fig. 6C**). Amoeboid morphology of the microglial cells suggests phagocytic saturation of the cell and it can no longer survey for any damage and cannot engulf more material for phagocytosis. Lyso-PS is found to play a role in phagocytosis; hence it was intuitive that unchecked lyso-PS levels in ABHD12 KO mice brain lead to the higher degree of phagocytosis by microglial cells. To confirm excessive phagocytosis by microglial cells in the ABHD12 KO mice brain we stained for LAMP1 – a phagocytosis marker in brain sections of LPS treated WT and ABHD12 KO mice along with their vehicle treated controls. Basally, in mice 8-10 weeks of age, we didn't find any changes in expression of LAMP1 protein in the microglial cells of vehicle treated ABHD12 WT and KO mice (**Fig. 6D,E**). But, there was significant increase in LAMP1 expression in microglial cells of both WT and ABHD12 KO mice immune challenged with LPS (**Fig. 6D,E**). Interestingly, ABHD12 KO microglial cells accumulated more LAMP puncta following LPS treatment compared to their LPS treated WT littermates (**Fig. 6D,E**). It was interesting to ask if elevated lyso-PS brings about the aberrant (rather elevated) phagocytosis by microglial cells in the ABHD12 KO mice following immune challenge with LPS. In order to test this, we measured the lipids involved in the ABHD16A–ABHD12 metabolic axis i.e., PS and lyso-PS. In addition to PS and lyso-PS, we also measured oxidized PS (ox-PS) in the brain as they are reported to be elevated in dying cells due to the oxidative stress caused by immune challenge and inflammation. We checked if PS or lyso-PS levels change in the mice brain following immune challenge with LPS. We didn't find any changes in lyso-PS or PS levels following immune challenge (**Fig. 6F,G**). To confirm that excess lyso-PS produced on inflammation was not degraded by ABHD12 in my

experimental time scales and since increased phagocytosis was seen in ABHD12 KO mice brain, we measured their levels in immune challenged ABHD12 KO mice. Unfortunately, ABHD12 KO mice too we didn't find any change in lyso-PS

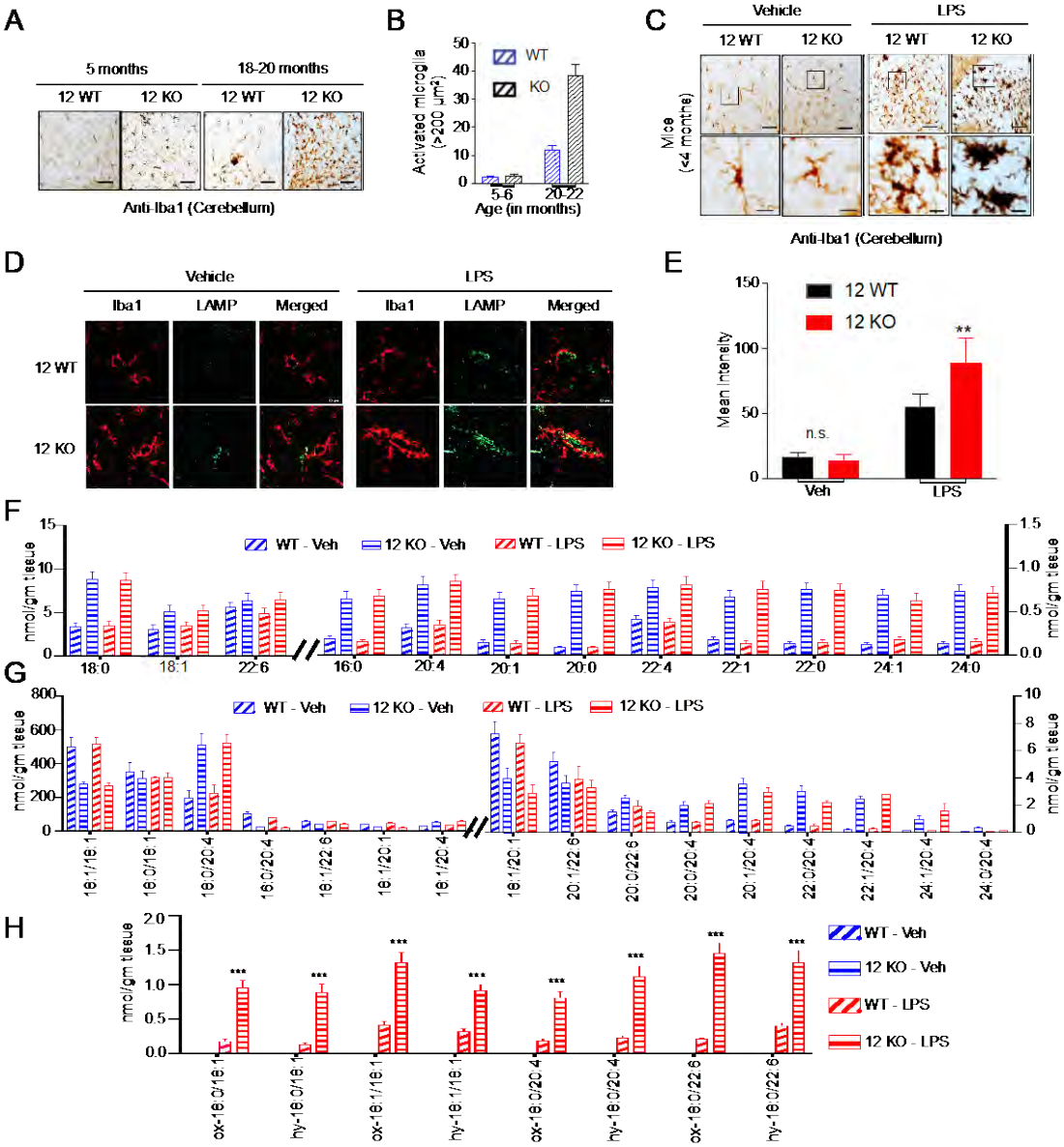

Fig. 6: ABHD12 activity regulates phagocytosis by microglial cells in the brain possibly through oxidized phosphatidylserine signaling. A – Representative image of microglial cells (anti-Iba1) in WT and ABHD12 KO mice cerebellum of different age groups. B – Quantification of activated microglial cells in the cerebellum of WT and ABHD12 KO mice. C – LPS treatment robustly activate microglial cell across genotype and ABHD12 KO mice shows amoeboid microglial cell morphology following LPS treatment. D – ABHD12 KO microglial cells show higher LAMP1 expression in the brain post LPS administration. E – Quantification of LAMP1 intensity in the microglial cells. F – Lyso-PS levels don't change in the brain of WT or ABHD12 KO mice post LPS treatment. G – PS levels don't change in the brain of WT or ABHD12 KO mice post LPS treatment. H – ABHD12 KO mice brain accumulated 2-3 fold higher ox-PS following

*LPS treatment compared to the LPS treated WT mice. Data plotted as mean ± standard deviation. Student's t-test (two-tailed): **P<0.01, ***P<0.001, ****P<0.0001.*

or PS levels as a function of LPS treatment (**Fig. 6F,G**). Though, in comparison to WT mice ABHD12 KO mice accumulated 4-5 more lyso-PS but it was independent of immune challenge with LPS treatment (**Fig. 6F,G**). Next, we measured the ox-PS and LPS treated mice showed elevated ox-PS levels in their brain. We could not find any differences in the ox-PS levels basally in the brain of ABHD12 WT and ABHD12 KO mice. Interestingly, ABHD12 KO mice showed several fold higher ox-PS levels in the brain following LPS treatment compared to that of LPS treated WT mice (**Fig. 6H**). Further work done with others in the lab (including chemical genetic screen, cellular and biochemical characterization of ABHD12) successfully annotated ABHD12 as an ox-PS lipase (data not shown here). It is interesting finding that suggests that ABHD12 can possibly regulate ox-PS in the mammalian systems with a special emphasis to its role as eater of eat me signal itself (i.e. ox-PS), thus protecting the cells from unwanted phagocytosis. Its likely that elevated phagocytosis by microglial cells in the LPS treated ABHD12 KO mice due to excessive accumulation of ox-PS under the conditions of oxidative stress induced by immune challenge.

Lyso-PS activates microglial cell basally in the brain of ageing ABHD12 KO mice. Once, ABHD12 was annotated as the ox-PS lipase and ox-PS was accumulated in brain under the conditions of oxidative stress, an another interesting question that arose was whether activated microglial cells in the ageing ABHD12 KO mice brain was due to accumulated lyso-PS or ox-PS. Though, we didn't find any ox-PS accumulation in the ABHD12 KO mice brain basally, there is always a very chance of ox-PS accumulation in ABHD12 KO mice below the limit of quantification/detection of the mass spectrometer. To check on this, if we revisit lyso-PS metabolism in the mammalian brain, it is synthesized by ABHD16A. Loss of ABHD12 activity fails to degrade the lyso-PS flux coming from ABHD16A activity, thus causing lyso-PS build up. If one can ablate ABHD16A activity in ABHD12 KO mice, in principle it should substantially reduce the levels of lyso-PS in the neural tissues of ABHD12 KO mice. If microglial cells were activated due to elevated lyso-PS, ABHD16A disruption should alleviate microglial cell activation and neuro-inflammation. With this logic, we created double knockout mice i.e., ABHD16A KO ABHD12 KO mice and examined their microglial cell once they were more than 1 year old. We didn't find any morphological differences in microglial cells of ABHD16A KO mice. ABHD12 KO mice >1 year in age showed an increased number of activated microglial cells as reported previously (**Fig. 7 A,B**).

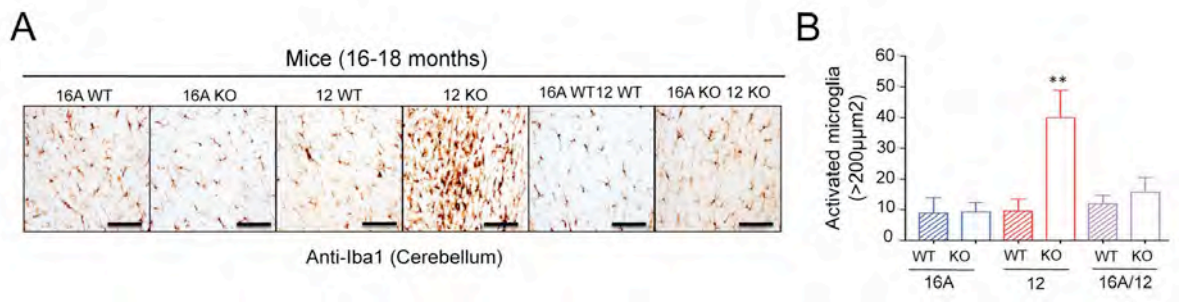

*Fig. 7: Microglial cell activation of ABHD12 KO mice is ablated in ABHD16A KO ABHD12 KO mice. A – Representative image of microglial cell (anti-Iba1 stained) in the cerebellum of WT, ABHD16A KO, ABHD12 KO, ABHD16A KO ABHD12 KO mice. B – Quantification of activated microglial cells in mice brain of different genotype older than 1 year. Data plotted as mean ± standard deviation. Student's t-test (two-tailed): **P<0.01, ***P<0.001, ****P<0.0001.*

Interestingly, in case of ABHD16A/ABHD12 double knock out mice there was no atypical activation of microglial cells in contrast to what is observed in ABHD12 KO mice (**Fig. 7A,B**). It means that microglial cell activation seen on loss of ABHD12 was alleviated by ablation of lyso-PS synthetic enzyme ABHD16A (**Fig. 7A,B**). It strongly suggests that microglial cell activation in ABHD12 KO mice basally was due to defective lyso-PS signaling.

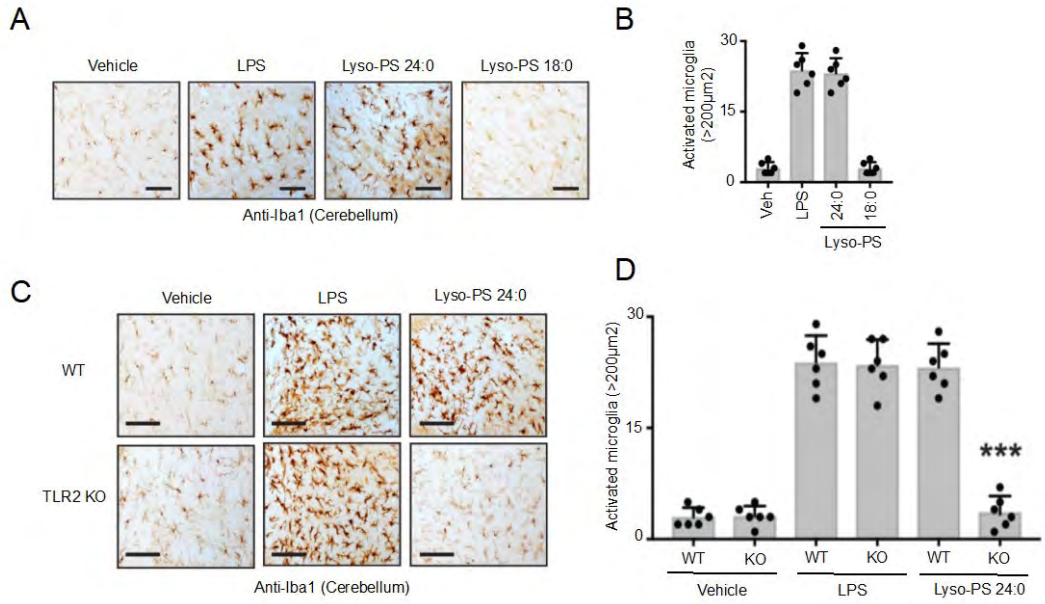

*Fig. 8: Very long chain lyso-PS activates microglia in Toll like receptor 2 (TLR2) dependent manner. A – Very long chain lyso-PS like lyso-PS 24:0 activates microglial cells (anti-Iba1) with equal propensity to LPS but long chain lyso-PS like lyso-PS 18:0) fails to activate microglial cells. B – Very long chain lyso-PS 24:0 fails to activate microglial cells in TLR2 KO mice. Data plotted as mean ± standard deviation. Student's t-test (two-tailed): **P<0.01, ***P<0.001, ****P<0.0001.*

Long chain lyso-PS activates microglial cell through Toll like receptor 2 (TLR2). Double knock out studies suggested that lyso-PS could be a potent signaling molecule that activates microglial cells. To confirm this, we tested if lyso-PS injection could activate microglial cells and trigger neuro-inflammation in the mice brain. We tested two lyso-PS species – one long chain lyso-PS 18:0 and one very long chain lyso-PS 24:0. We administered these through intravenous (I.V.) route to WT mice and monitored their response by probing their pain phenotype and microglia. At dose of 1 mg/kg intravenous (I.V.), long chain lyso-PS 18:0 didn't show any visible pain phenotype but lyso-PS 24:0 triggered visible immune stress and pain phenotype (orbital tightening, nose bulging, cheek bulging, reduced or negligible motor

activity, shivering, etc.). We probed for microglial cell in these mice and found that there was increased microglial cell activation following very long chain lyso-PS 24:0 injection. The number of activated microglial cells post lyso-PS 24:0 injection was comparable to numbers seen post LPS treatment, suggesting that lyso-PS 24:0 acts almost as good antigen as LPS (**Fig. 8A,B**). Long chain lyso-PS 18:0 didn't show any changes in microglial cell activation when compared to vehicle (PBS) treated mice (**Fig. 8A,B**). We found these observations to be true for all regions of brain investigated including cerebellum, cortex and hippocampus (**data not shown**). This suggests that very long chain lyso-PS can activate microglial cells to cause neuro-inflammation but long chain lyso-PS cannot. Next, we started to screen for receptors through which very long chain lyso-PS activated microglial cells. Based on screening in literature, we chose TLR2 as a possible receptor as it was highly expressed in microglial cells and was not investigated ever before in context to lyso-PS induced neuro-inflammation, and there were some reports of TLR2 as a receptor for lyso-PS in worms. TLR2 KO mice basally didn't show any changes in the morphology or number of microglial cells. We injected TLR2 KO mice with LPS and lyso-PS 24:0 LPS treated TLR2 KO mice showed microglial cell activation comparable to what is seen in WT mice. Interestingly, lyso-PS 24:0 treatments to TLR2 KO didn't trigger any microglial cell activation in the brain (**Fig. 8C,D**) in contrast to robust microglial cell activation seen in lyso-PS 24:0 injected WT mice (**Fig. 8C,D**). Cytokine measurements from the microglial and peritoneal macrophages as well showed the similar trend (data not shown), strongly suggesting that TLR2 is a receptor for very long chain lyso-PS in the mammalian physiology. Thus, loss of ABHD12 leads to accumulation of very long chain lyso-PS in the CNS, which in turn causes neuro-inflammation through TLR2 receptor.

Minocycline can alleviate neuro-inflammation in ABHD12 KO mice. After establishing that lyso-PS causes neuro-inflammation in the ABHD12 KO mice, we started to look for small molecules that can alleviate the neuro-inflammation seen in ABHD12 KO mice. We found minocycline hydrochloride – a tetracycline antibiotic but robustly shown to deplete microglial cells and reduce cytokine secretion from macrophages. We found that minocycline administration every day for 4 weeks could successfully reduce the number of activated microglial cells in ABHD12 KO mice older than a year and it is it is likely that minocycline reduced neuroinflammation in ABHD12 KO mice by inhibiting cytokine secretion induced through accumulated very long chain lyso-PS signaling (**Fig. 9**).

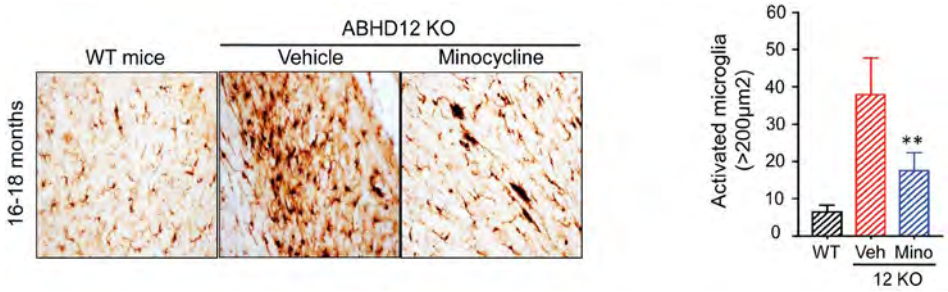

Fig. 9: Minocycline administration reduces number of activated microglia in the ABHD12 KO mice brain. A – Representative image of cerebellar microglia (anti-Iba1) and quantification of activated microglia in

*the cerebellum. Data plotted as mean ± standard deviation. Student's t-test (two-tailed): **P<0.01, ***P<0.001, ****P<0.0001.*

Discussion

PHARC syndrome is an age dependent genetically recessive neurological disorder presumed to be caused by deregulated lipids in the brain, principally lyso-PS. Mice models of PHARC i.e., ABHD12 knock out (KO) mice accumulate lyso-PS in the neural tissues, followed by elevated microglial activation (neuro-inflammation) and sensory motor defects like hearing loss, ataxia and poor coordination, similar to what is observed in PHARC human subjects. But the molecular mechanism through loss of ABHD12 activity brings about PHARC pathophysiology was largely unknown and under investigated. Here, we tried to map the metabolic flux of lyso-PS in the mammalian neural cells and so as to better understand the dynamics cellular of lyso-PS pools. Firstly, we developed protocols to purify and biochemically characterize lyso-PS biosynthetic enzyme ABHD16A. My biochemical studies show that ABHD16A acts as a PS specific PLA_2 enzyme and generates sn-2 lyso-PS, which is an established signaling molecule in the mammalian peripheral tissues. Next, we showed that both ABHD16A and ABHD12 regulate lyso-PS level from the ER in the mammalian cells. From the literature, it was known that PS is synthesized by phosphatidylserine synthase 1 and phosphatidylserine synthase 2 at the mitochondrial associated membranes (MAMs) in the mammalian cells. PS synthesized at MAMs takes three metabolic routes, firstly, it is fluxed to mitochondria where it is transformed to PE by PS decarboxylase. Secondly, PS is transported to plasma membrane in exchange of phosphatidylinositol 4-phosphate using oxysterol binding protein related protein 5/8. Lastly, PS participates in vesicular trafficking by being an active part of the cellular vesicles and it reaches to other organelle membranes. My studies here provide a new metabolic route for PS, where PS is metabolized by ABHD16A at ER to lyso-PS. Notably, ABHD16A is first intracellular mammalian PS lipase. Lyso-PS made at ER is further degraded by ABHD12 to glycerophosphoserine and FFA. Taken together ABHD16A and ABHD12 regulate lyso-PS flux from the ER in the mammalian cells (**Fig. 10**).

Having subcellular localization of ABHD16A and ABHD12 mapped, we moved on to probe for these proteins in different anatomical regions of the adult mice brain. We showed that ABHD16A expression was several fold higher in cerebellum of the mice brain whereas ABHD12 was pretty much ubiquitous across brain regions. Consistent with this observation, we also found that loss of ABHD16A or ABHD12 has major disturbances in lyso-PS levels in the cerebellum of the adult mice brain. This observation was interesting to the fact that cerebellum is the regions which undergoes age dependent degeneration (or atrophy) contributing to ataxia and motor defects in PHARC subjects. Next, we probed for ABHD16A and ABHD12 expression in the adult mice brain using immunohistochemistry and found that ABHD16A and ABHD12 are expressed on two different cerebellar layers that typically host different neuronal cells in the mice brain. ABHD16A was highly enriched on the granule neurons (granular layer) while ABHD12 was almost exclusively expressed in the Purkinje neurons (ganglionic layer) of the cerebellum. It made me hypothesize that lyso-PS could acts as a paracrine-signaling molecule between granule neurons and

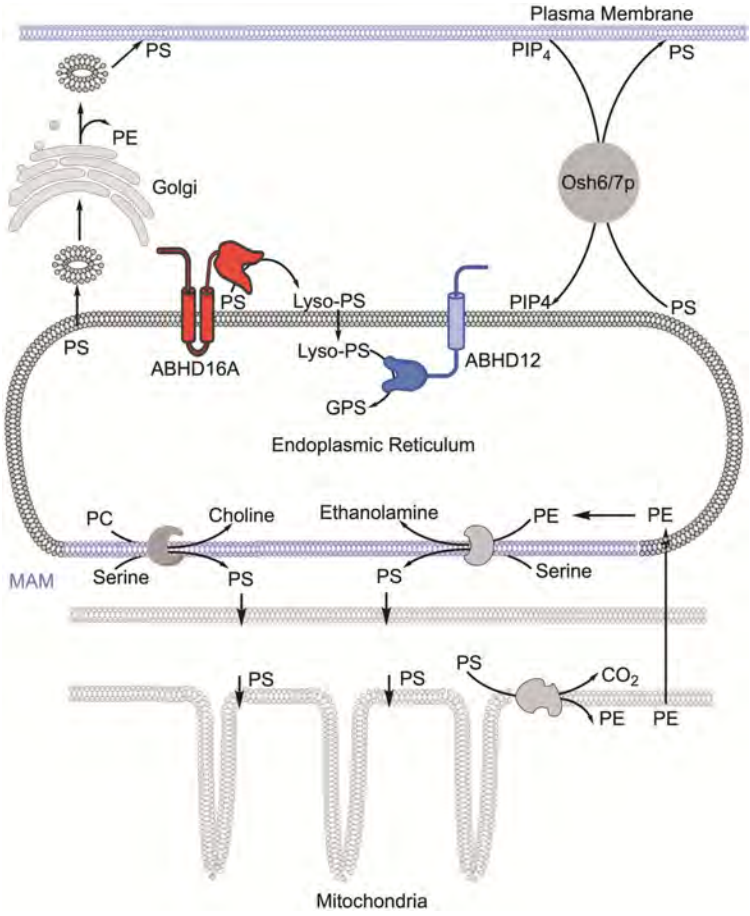

Fig.10: ABHD16A and ABHD12 regulate lyso-PS metabolism and flux from ER in endoplasmic reticulum. MAM = Mitochondrial associated membrane, PSS1 = Phosphatidylserine synthase 1, PS*S2 = Phosphatidylserine synthase 2*, *PSD = Phosphatidylserine decarboxylase, ORP5/8 = Oxysterol-binding protein related protein 5/8.*

Purkinje neurons of the cerebellum in the mammalian brain. Using several parallel approaches, we showed that lyso-PS secreted from granule neurons induce phosphorylation of ERK1/2 in the Purkinje neurons, thus strongly suggesting that granule neurons and Purkinje neurons cross talk using lyso-PS as one of the signaling molecule (**Fig. 11**). Further investigations using lyso-PS library lead to the observation that long chain lyso-PS species (like lyso-PS 18:0) is most potent in inducing phosphorylation of ERK1/2.

ABHD12 KO mice show lyso-PS build up and elevated microgliosis (activated microglial cells and neuro-inflammation) in an age dependent manner suggesting some role of ABHD16A – ABHD12 – lyso-PS in the neuro-immunophysiology of mammalian brain. We found that loss of ABHD12 activity leads to elevated phagocytosis by microglial cells thus causing deregulated injury to the neural tissues. Further investigations lead to the establishment that ABHD12 acts as an oxidized PS lipase, which is a signaling molecule for phagocytosis. Thus, it is likely that elevated phagocytosis by microglial cells in ABHD12 KO mice is driven by accumulated oxidized PS under the conditions of oxidative stress. Next, we checked if basal neuro-inflammation in ABHD12 KO mice contributed by lyso-PS or ox-PS. To test this, we generated ABHD16A and ABHD12 double knock out mice that had rescued levels of accumulated lyso-

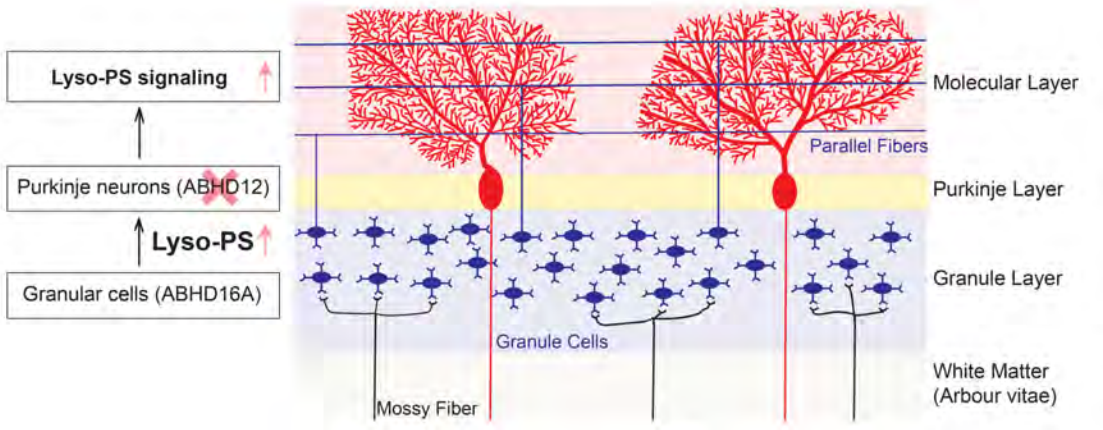

Fig.11: Paracrine signaling model for lyso-PS signaling in the cerebellum regulated by ABHD16A and ABHD12 enzymatic activities.

PS in the brain. Interestingly, double knock out mice older than 1 year didn't show any microglial activation or neuro-inflammation suggesting that lyso-PS is the metabolite that triggers neuro-inflammation in ABHD12 KO mice. To confirm this, we administered mice with lyso-PS and we found that very long chain lyso-PS like lyso-PS 24:0 activates microglia through Toll like receptor 2 (TLR2). To bring down the neuro-inflammation in the ABHD12 KO mice, we screened a set of small molecules and found that minocycline administration for a few weeks could successfully alleviate the neuro-inflammation in the ABHD12 KO mice (**Fig. 12**).

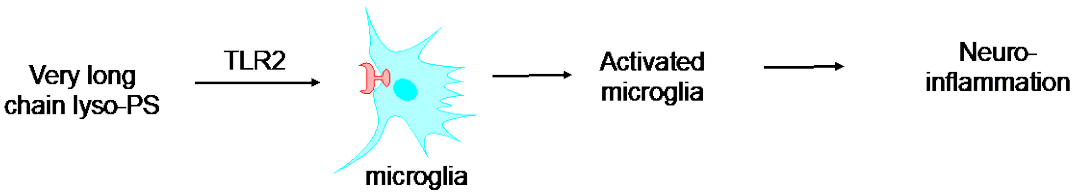

Fig.12: Very long chain lyso-PS activates microglial cells through TLR2 receptor and cause neuroinflammation.

Overall, we successful demonstrate that long chain lyso-PS like lyso-PS 18:0 acts as a signaling molecule in the neurons through some unidentified receptor whereas very long chain lyso-PS like lyso-PS 24:0 signals through TLR2 to activate microglial cells leading to neuro-inflammation. My work described in this thesis elegantly establish that ABHD16A and TLR2 can be a good therapeutic target to alleviate neuro-inflammation in the ABHD12 KO mice and minocycline can be a promising small molecule candidate to manage neuro-inflammation.

Going ahead, it would be interesting to investigate if neuro-behavioral defects in ABHD12 KO mice arise due to lyso-PS triggered neuro-inflammation or its signaling role on Purkinje neurons in the cerebellum or may be both. To answer this, one should screen ABHD16A KO – ABHD12 KO mice, ABHD12 KO – TLR2 KO mice for sensory motor behavior, defects in which are seen in PHARC patients or PHARC

mice models. It also remains an interesting question to pursue how lyso-PS mediated granule neuron – Purkinje neuron communication drives the broader neurophysiological processes or behavioral output.

Conclusion

ABHD16A is a PS specific PLA_2 enzyme and it generates sn-2 lyso-PS lipids – an active signaling molecule in mammals. Both ABHD16A and ABHD12 (lyso-PS degradative enzyme) localize at ER and regulate lyso-PS from ER in the mammalian cells. Brain contains two types of lyso-PS species, namely long chain and very long chain lyso-PS lipids. Long chain lyso-PS acts as a potent signaling molecule between granule neuron and Purkinje neurons in the cerebellum of mice brain. Very long chain lyso-PS regulate innate immunity by activating brain macrophages (microglial cells) through TLR2 receptor. Neuroinflammation seen in ABHD12 KO mice (PHARC syndrome model organisms) can be successfully elevated by blocking ABHD16A activity, TLR2 receptor and by administering small molecule minocycline. The findings described here provide novel insights into lyso-PS biology and pathophysiology of PHARC syndrome, and also they provide a few promising therapeutic intervention strategies to manage PHARC Syndrome.

d) Impact of research in the advancement of knowledge

First, our studies provide a benchmark of strategies to study age dependent neurological disorders using a diverse array of tools like – protein purification, enzymology, animal experiments, microscopy and mass spectrometry-based metabolomics. It describes the development of new methods to purify lipases and quantify lipids from mammalian tissues. They all can be applied to investigate new research question. We also provide basic mechanistic insights into lyso-PS lipid metabolism and signaling in the mammalian central nervous system. We provide molecular details of the PHARC pathophysiology that helps us better understand PHARC. Towards therapeutic side, we show that ABHD16A and/or TLR2 inhibition helps in alleviating the neuroinflammation seen in the PHARC Syndrome. Thus, discovery of better inhibitors can be built as therapeutic drugs for PHARC Syndrome. We also show that minocycline (a FDA approved drug already available on medical counters) successfully and robustly reduced the neuroinflammation associated with PHARC Syndrome. Thus, minocycline can also be explored further as drug to manage PHARC Syndrome.

References

1 Yoshimura, H. *et al.* Novel ABHD12 mutations in PHARC patients: the differential diagnosis of deaf-blindness. *Ann Otol Rhinol Laryngol* **124** Suppl 1, 77S-83S, doi:10.1177/0003489415574513 (2015).

2 Tingaud-Sequeira, A. *et al.* Functional validation of ABHD12 mutations in the neurodegenerative disease PHARC. *Neurobiol Dis* **98**, 36-51, doi:10.1016/j.nbd.2016.11.008 (2017).

3 Nishiguchi, K. M. *et al.* Exome sequencing extends the phenotypic spectrum for ABHD12 mutations: from syndromic to nonsyndromic retinal degeneration. *Ophthalmology* **121**, 1620-1627, doi:10.1016/j.ophtha.2014.02.008 (2014).

4 Lerat, J. *et al.* A complex homozygous mutation in ABHD12 responsible for PHARC syndrome discovered with NGS and review of the literature. *J Peripher Nerv Syst* **22**, 77-84, doi:10.1111/jns.12216 (2017).

5 Blankman, J. L., Long, J. Z., Trauger, S. A., Siuzdak, G. & Cravatt, B. F. ABHD12 controls brain lysophosphatidylserine pathways that are deregulated in a murine model of the neurodegenerative disease PHARC. *Proc Natl Acad Sci U S A* **110**, 1500-1505, doi:10.1073/pnas.1217121110 (2013).

6 Kamat, S. S. *et al.* Immunomodulatory lysophosphatidylserines are regulated by ABHD16A and ABHD12 interplay. *Nat Chem Biol* **11**, 164-171, doi:10.1038/nchembio.1721 (2015).